THERMOSTRUCTURAL ANALYSIS OF A SCRAMJET FUEL-INJECTION STRUT

Allan R. Wieting
NASA Langley Research Center

and

Earl A. Thornton
Old Dominion University

THERMOSTRUCTURAL ANALYSIS OF A SCRAMJET FUEL-INJECTION STRUT

Allan R. Wieting
NASA Langley Research Center

and

Earl A. Thornton
Old Dominion University

INTRODUCTION

AIRFRAME-INTEGRATED SCRAMJET

(Figure 1)

Studies of airframe-integrated scramjets with high potential performance led to the sweptback, fixed-geometry, hydrogen-fueled, rectangular scramjet module shown in figure 1. Two inner scramjet modules are shown; the sidewall of one module is removed to reveal the internal engine surfaces. The scramjet modules are integrated with the airframe and use the entire undersurface of the aircraft to process engine airflow. The aircraft forebody serves as an extension of the engine inlet, and the afterbody serves as an extension of the engine nozzle. Discussion of the propulsion aspects of this scramjet concept can be found in the paper by Jones (ref. 1).

A preliminary thermal/structural design analysis study (ref. 2) based on Hypersonic Research Engine (HRE) technology (ref. 3) indicated viability from both an engine structural mass and coolant requirement standpoint. This study revealed a number of critical areas (e.g., panel-to-panel seals, fuel injection struts) and reemphasized the need for advances in fabrication and materials technology to obtain reasonable structural life.

Recently, a more detailed study (ref. 4) of this scramjet concept was undertaken by a major engine manufacturer while the effort at Langley concentrated on the fuel-injection struts. The primary function of the three fuel-injection struts is to provide the mechanism for multiplanar fuel injection into the supersonic airstream. Salient features from the thermal/structural design and analysis of the struts are presented in this paper.

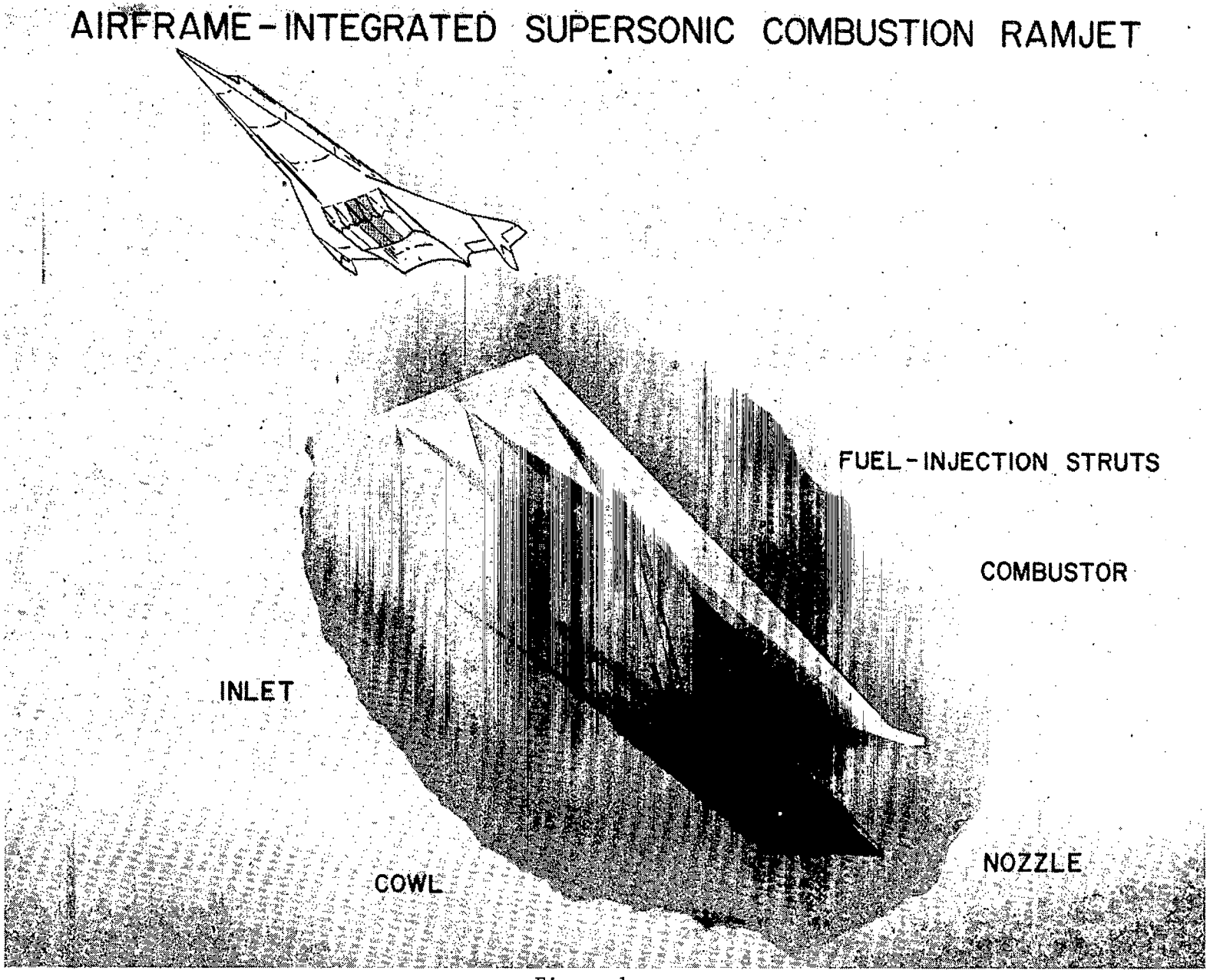
AIRFRAME - INTEGRATED SUPERSONIC COMBUSTION RAMJET
FUEL - INJECTION STRUTS
COMBUSTOR
INLET
NOZZLE
COWL

Figure 1

STRUT GEOMETRY AND AEROTHERMAL ENVIRONMENT

(Figure 2)

The struts, which are shown in figure 2, have a slender wing-like configuration. The struts are swept back 48° and span the distance between the engine top wall and cowl. An axial cross section at any spanwise location along the sweep line is shown in the upper right figure. The center strut is symmetric and the two side struts are asymmetric. The side strut thickness is approximately 7 percent of the chord; the chord is approximately 45 percent of the span. The struts are immersed in the supersonic flow, partially in the inlet and partially in the combustor and therefore are exposed to a hostile environment.

The thermal environment is characterized by the chordwise heat flux $\dot{q}$ distribution along both sides of the strut shown in the lower left figure. The heating is highly nonuniform because of stagnation, shock boundary-layer interaction, and combustion. The heat flux which varies by an order of magnitude is also asymmetric.

STRUT GEOMETRY AND THERMAL ENVIRONMENT

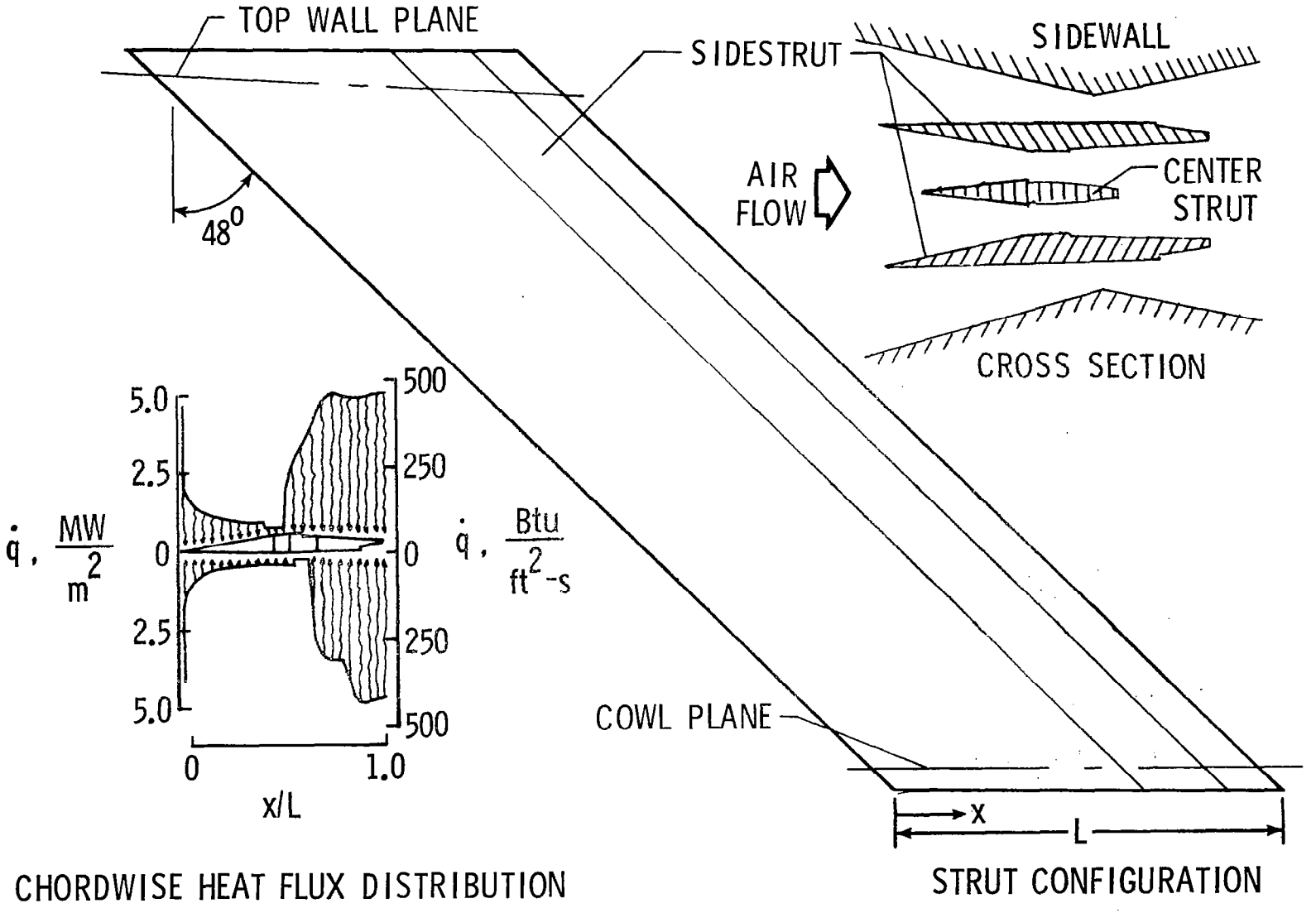

Figure 2

STRUT CONSTRUCTION

(Figure 3)

The struts must simultaneously support a large side load, contain high-pressure hydrogen at two temperature extremes, and withstand high thermal stresses resulting from complex aerodynamic heating as well as convective heating from the hot hydrogen in the internal manifolds. To compound the design problem, the cross-sectional area and contour cannot be altered without significantly changing the engine propulsion performance.

Each strut is subdivided internally into four longitudinal compartments by three major bulkheads as shown in the figure. The fore and aft compartments serve as coolant inlet and outlet manifolds, respectively, and the central compartments serve as fuel manifolds for the strut trailing edge (parallel to airflow) and wall (perpendicular to airflow) fuel injectors. Coolant in the inlet manifold is injected through a slot, impinges on the leading edge, and splits (unequally) to flow along each wall to the trailing edge, where it is collected in the outlet manifold. This quadrilateral manifold configuration was selected over a more structurally efficient (high pressure containment) tubular configuration because the former has a greater volumetric efficiency which results in larger fuel and coolant flow areas and thus lower pressure losses. Structural details are shown in the lower figure. The primary structure is basically a 2.5 mm (.1 in.) thick wall. Normally, internal convective heating from the hot hydrogen in the manifolds would be negligible compared to the aerodynamic heating. However, because of the higher velocities caused by the still restricted flow area, internal convective heating is significant. A metallic plate-fin thermal buffer, with the fins oriented transverse to the fuel flow direction to restrict flow and provide essentially stagnant hydrogen in the passages between the shield and the strut wall, eliminates direct convective heating to the strut wall. A pin fin coolant passage is used on the external surfaces. Hydrogen coolant routed through the passage absorbs the aerodynamic heat load.

STRUT CONSTRUCTION

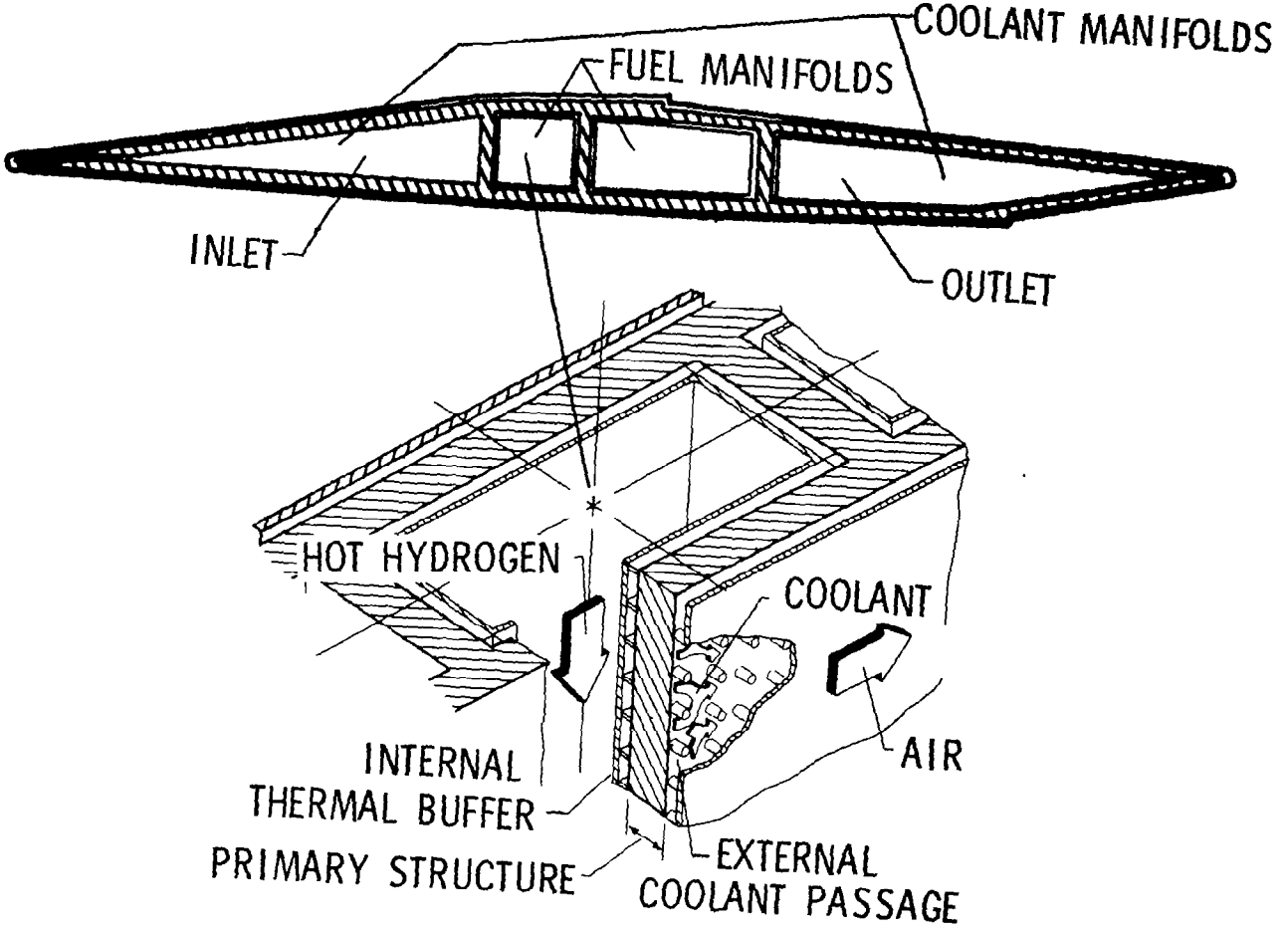

Figure 3

DESIGN TEMPERATURE LOADS

(Figure 4)

The design temperatures are characterized by the chordwise temperature (T) distributions shown in the figure for the starboard structural wall of the strut. The temperature distributions along the port wall are similar. The solid line indicates the wall temperature adjacent to the coolant passage, and the dashed line indicates the wall temperature adjacent to the manifold. The solid symbols denote the average temperature of the major bulkheads. During operation the forward section is below ambient, and the aft section is above ambient. Significant thermostructural loads result from the nonlinear chordwise temperature gradient and the transverse temperature gradients through the walls and bulkheads. The chordwise temperature gradient is caused by the highly non-uniform aerothermal heating (fig. 2), and the transverse gradients by the internal convective heating.

DESIGN TEMPERATURE LOADS

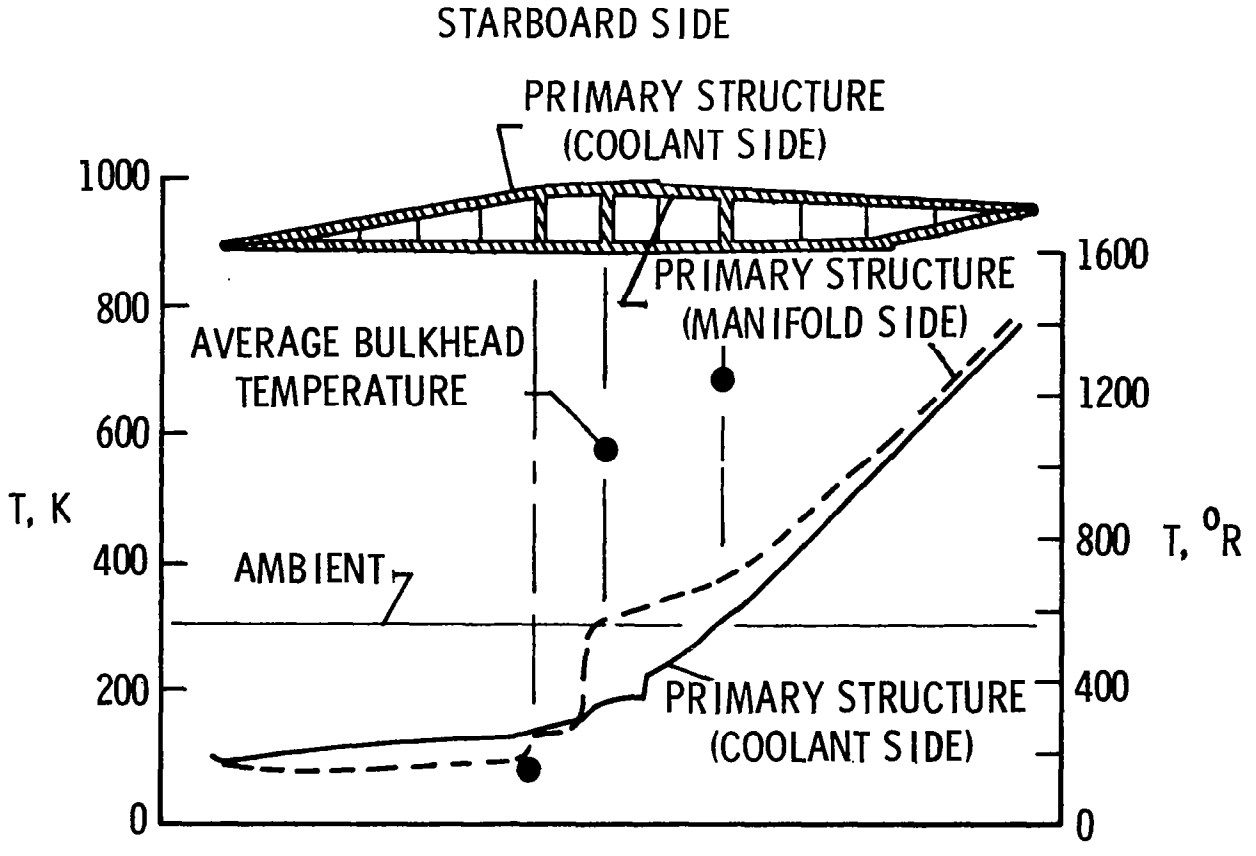

Figure 4

ATTACHMENT SCHEME AND DEFORMATIONS DUE TO CHORDWISE TEMPERATURE GRADIENT

(Figure 5)

Overall thermal expansions of the strut are accommodated by the mounting system shown schematically in the left figure. The strut top wall and cowl mounts are approximately at mid-chord. At the top the strut has rotational freedom about the pin axis and translational freedom fore and aft from the pin. At the cowl the strut has rotational freedom about all axes and translational freedom along the 48° sweep line.

The deformations due to the nonlinear chordwise temperature gradient are primarily in the spanwise plane as shown schematically in the right figure. The leading edge shrinks and the trailing edge expands, causing bending about the spanwise axes. The maximum deflection in the chordwise direction is 3.0 mm (0.12 in.) and is the result of bending caused primarily by the chordwise temperature gradient. The bending of the strut causes local changes in the sweep angle. The local sweep angle change along the leading and trailing edge is between 1 to -2 degrees. The radius of curvature which defines the local angle change, can be approximately by $r = w/\alpha\Delta T$ where w is the perpendicular distance between leading and trailing edge, α is the coefficient of thermal expansion, and ΔT is the chordwise temperature difference. The maximum deflection in the spanwise direction (4.3 mm (0.17 in.)) is at the trailing edge at the cowl plane and is caused primarily by the increase in the trailing edge temperature above ambient (ΔT = 550 K (ΔT = 1000°F)). These deformations are critical to the seal design at the top wall and the cowl. The cowl seal is particularly critical because the strut leading edge overhangs the cowl leading edge and the aft section of the strut penetrates the cowl.

ATTACHMENT SCHEME AND DEFORMATIONS DUE TO CHORDWISE TEMPERATURE GRADIENT

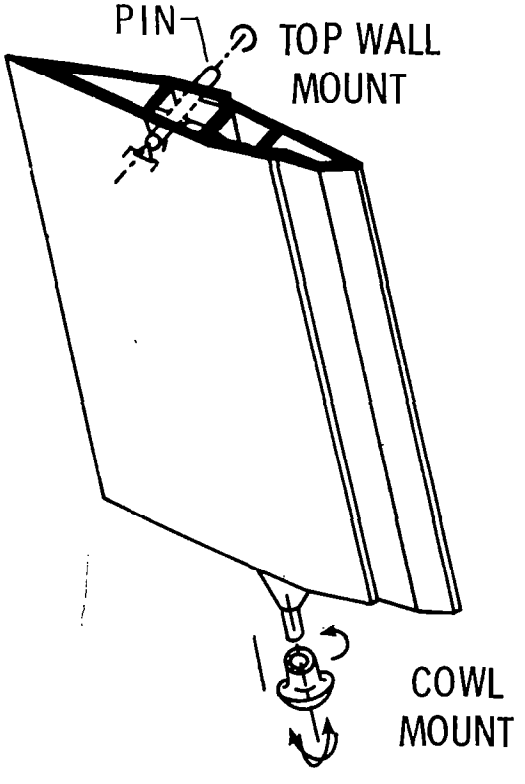

ATTACHMENT SCHEME

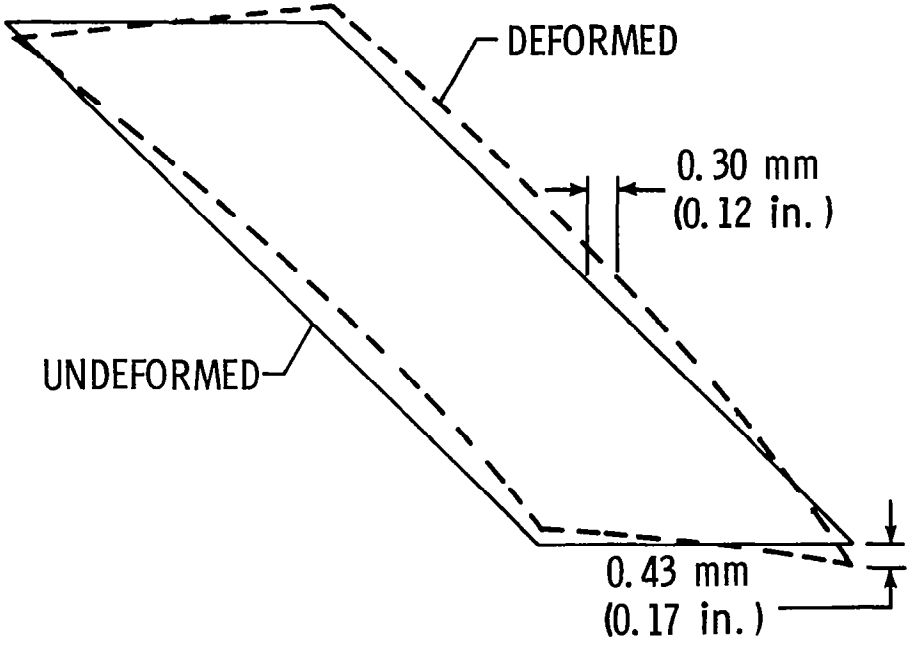

IN PLANE DEFORMATIONS
(NOT TO SCALE)

Figure 5

STRESSES DUE TO CHORDWISE TEMPERATURE GRADIENT

(Figure 6)

As shown in the left figure, the stresses due to the nonlinear chordwise temperature gradient concentrate primarily in the rectangular midsection of the strut, leaving the ends relatively lowly stressed, which simplifies the attachment design. The principal stresses are basically aligned with the sweep which is indicative of the overall bending action in the spanwise plane. A chordwise distribution of the principal stress in the spanwise direction normalized by the allowable stress is shown in the right figure. As expected, the leading and trailing edges are in compression - with a maximum stress approximately 50 percent of the allowable - and the midsection is in tension - with a maximum stress of approximately 30 percent of the allowable. The results are typical for both walls.

STRESS DUE TO CHORDWISE TEMPERATURE GRADIENT

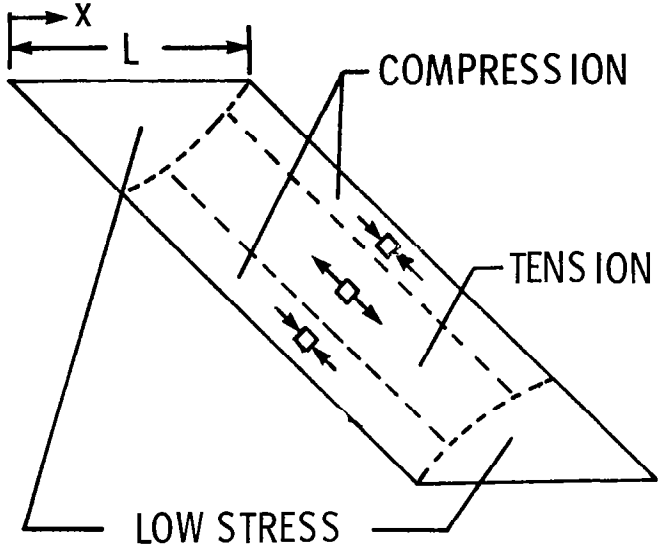

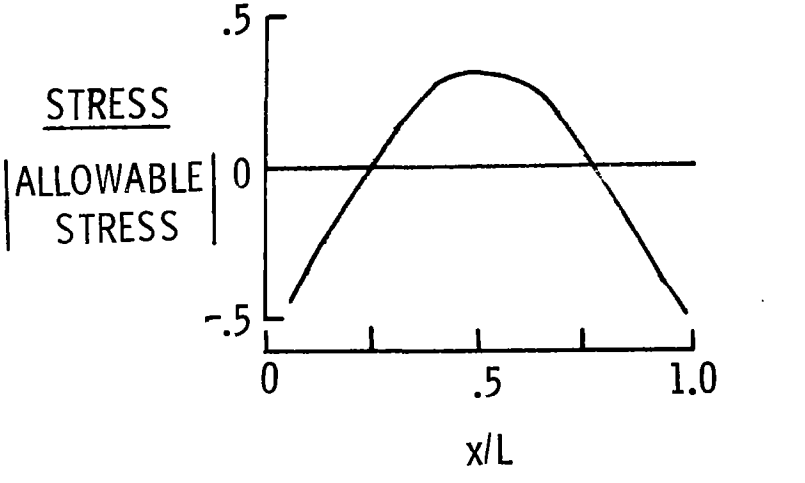

CHORDWISE STRESS DISTRIBUTION

- STRESSES UNIAXIAL
- STRESSES LOW IN MOUNT AREA

Figure 6

DEFORMATIONS AND STRESSES DUE TO TRANSVERSE TEMPERATURE GRADIENTS

(Figure 7)

The transverse temperature gradients primarily result from the internal convective heat transfer from the hydrogen in the manifolds although the asymmetric aerodynamic heating is also a contributor. The result of these heat loads is a wall gradient ΔT_W and a bulkhead gradient ΔT_B. These gradients result in local wall bending and the out of plane deformation illustrated in the left figure. The two solid lines are nodal lines (zero deflection) and the two shaded areas indicate the areas of maximum positive and negative deflection which are negligible at approximately 0.0076 mm (0.0003 in.).

The chordwise stress distribution (in extreme fiber) resulting from the transverse gradients is shown normalized to the allowable stress in the figure on the right. The solid line illustrates the stress distribution due to the overall transverse gradient ($\Delta T_B + \Delta T_W$). The maximum stress is about 50 percent of the allowable. The bulkhead gradient (ΔT_B) primarily causes local bending in the wall in the vicinity of the bulkhead. The dashed line illustrates the stress distribution due to the wall gradient (ΔT_W) only. The maximum stress due to ΔT_W occurs near midchord and is approximately 30 percent of the allowable. This gradient (ΔT_W) results in a biaxial stress through the wall and therefore the spanwise component will add to the stress from the chordwise temperature gradient.

The combined thermal stresses (not shown), which dominate the design, are approximately 60 to 80 percent of the allowable. The stresses due to the pressure load for normal engine operating conditions are approximately 20 percent of the allowable, yielding a combined stress of 80 to 100 percent of the allowable and therefore a thermal/structural concept that is feasible under normal operating loads. However, the maximum external pressure loads do not occur during normal engine operation.

DEFORMATIONS AND STRESSES DUE TO TRANSVERSE TEMPERATURE GRADIENTS

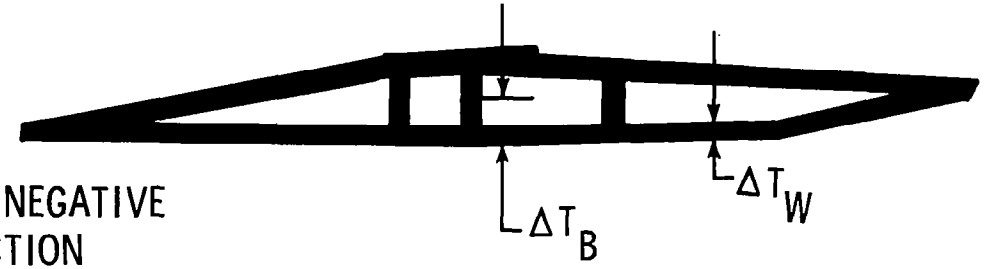

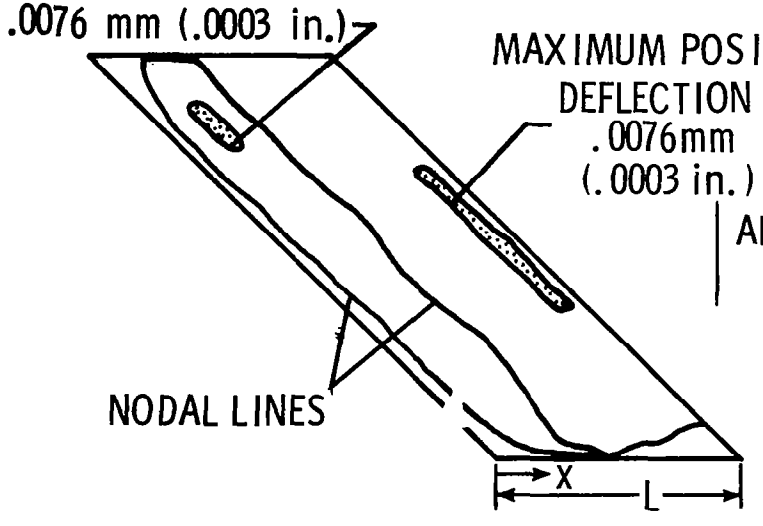

OUT OF PLANE DEFORMATION CONTOURS

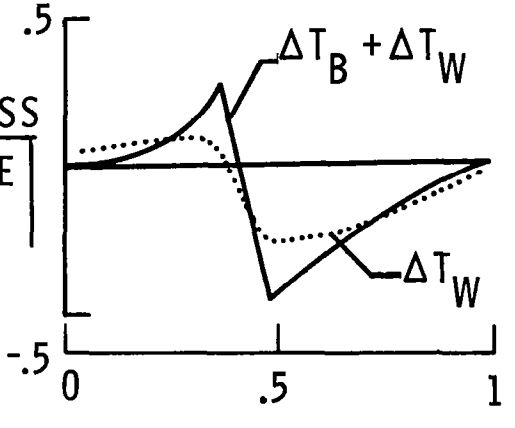

CHORDWISE STRESS DISTRIBUTION

Figure 7

CRITICAL PRESSURE LOADS

(Figure 8)

The maximum external pressure loads occur during an engine unstart (i.e., transition from supersonic to subsonic flow) which results if thermal choking occurs in the combustor. When the initial design study (ref. 2) was undertaken, the operational flow system was well understood; however, the unstarting process was not. Consequently, the basic unstart phenomena and loading were characterized experimentally (ref. 5). The maximum external pressure loading occurs at approximately Mach 5, when the aerodynamic flow in the passage between the sidewall and the side strut unstarts and the flow in the other three passages remains started as depicted in the upper left figure.

The unstarting process is highly transient as indicated by the shaded area on the typical pressure history shown in the right figure. The pressure is normalized to the steady state started pressure. The peak pressure occurs during the unstart and is an order of magnitude higher than the normal operating pressure and may be 2 to 7 times higher than the steady state unstarted pressure levels, which have typically been used in prior engine designs such as the HRE. These peak levels are conservatively predicted by normal shock wave theory. Since the complete dynamic characteristics of the transient pulse are not known, the envelope of the peaks along the strut currently serves as the basis for the structural design. The design pressure load isobars are shown schematically in the lower figure. Peak pressures are between 4.8 and 5.7 kPa (100 and 120 psi) over the majority of the strut.

CRITICAL PRESSURE LOADS

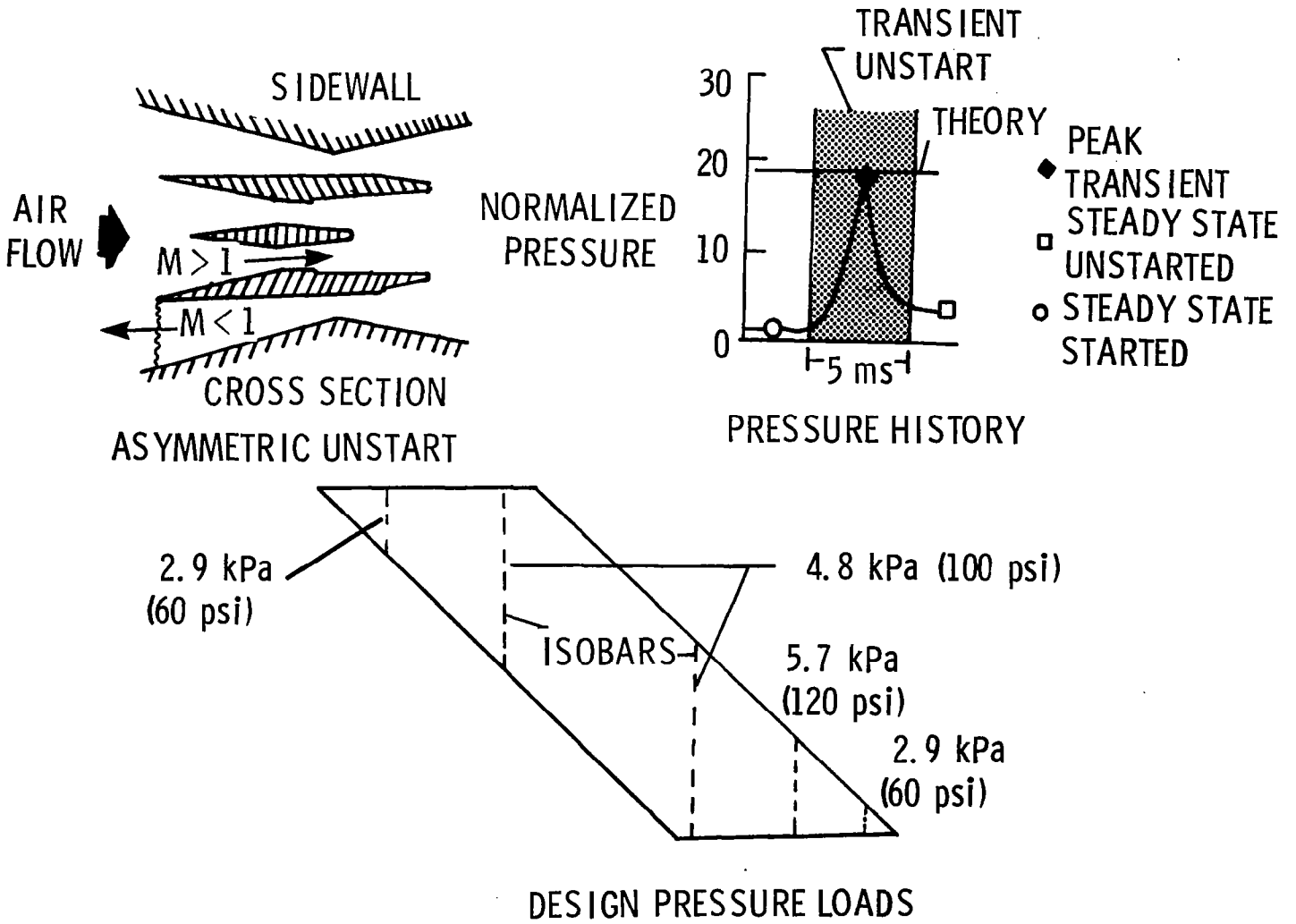

Figure 8

COMBINED STRESSES

UNSTART

(Figure 9)

Analytical results (refs. 2 and 4) indicate that the combined thermal and unstart pressure stresses exceed the allowable stress. As stated earlier the thermal stresses (60 to 80 percent of the allowable) are caused by the nonlinear chordwise temperature gradient and transverse temperature gradient shown in the left figure for a coolant outlet temperature (T_o) equivalent to the superalloy temperature limit of 890 K (1600°R). The temperature gradients are significantly reduced, as shown in the figure, by increasing the coolant flow to obtain an outlet temperature of 430 K (770°R). Attendant thermal stresses are reduced to approximately 30 percent of the allowable and the combined stresses are reduced approximately 50 percent to acceptable levels as shown in the right figure. Reducing the coolant outlet temperature yields a feasible strut concept and adds no complexity to the design or fabrication, and even though the strut coolant flow rate is doubled, the overall engine cooling requirement is increased only 5 percent. As discussed in reference 6, excess coolant is available at this flight condition. An alternate technique, identified in references 2 and 4, ties the three struts together at mid span; however, the tie greatly complicates cooling design and fabrication.

COMBINED STRESSES

UNSTART

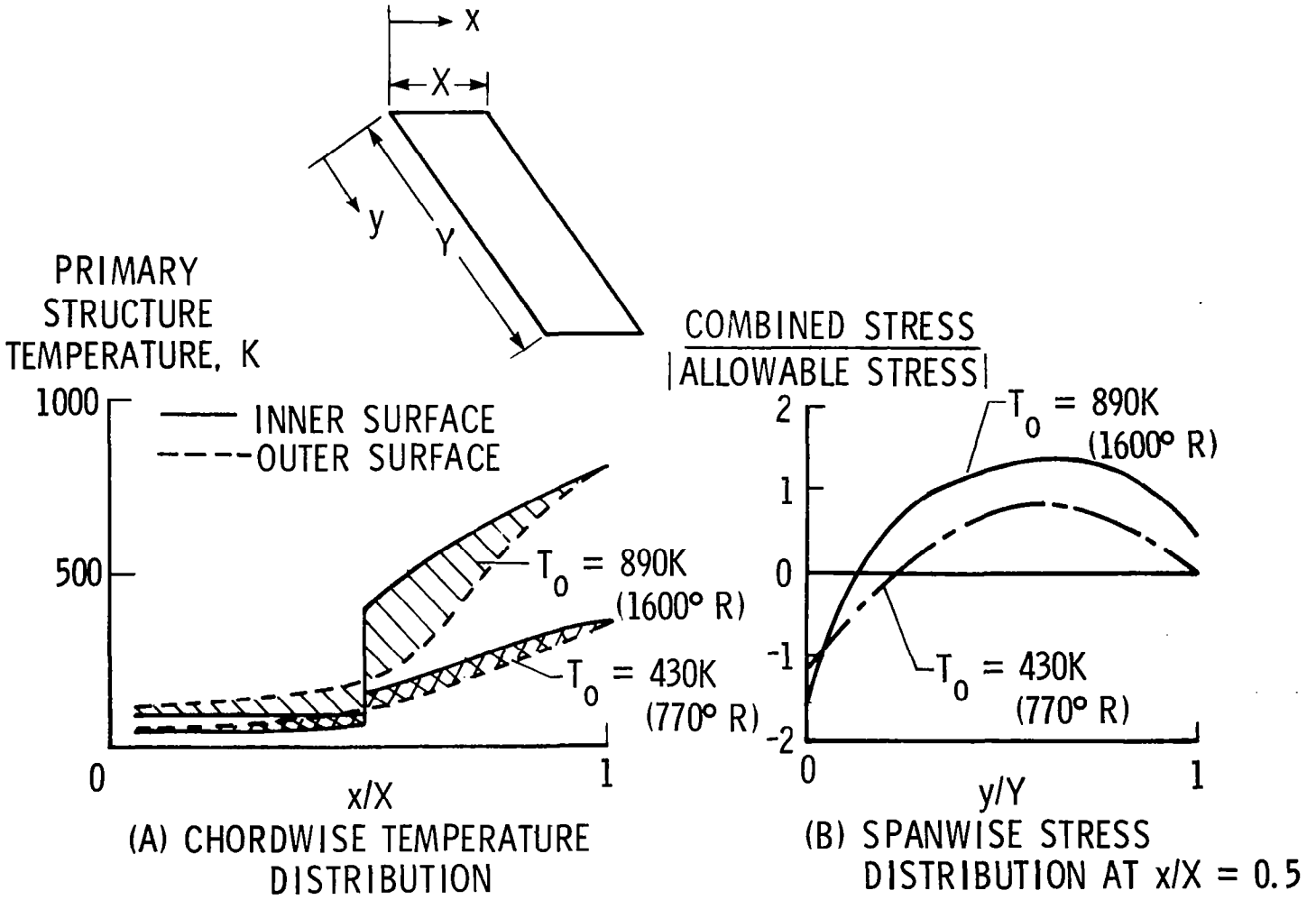

Figure 9

DEFORMATIONS DUE TO THE UNSTART PRESSURE

(Figure 10)

The out of plane deformations due to the unstart pressure load only are indicated by the contour plot shown in the figure. Overall deformation indicates a twisting action with the maximum chordwise deformations at mid span and a maximum deflection of approximately 1.5 cm (0.6 in.) at the trailing edge. Maximum displacements at the top wall and cowl planes are between 0.5 and 0.8 cm (0.2 and 0.3 in.) These deformations are considered a maximum as no constraint at the top wall and cowl planes was assumed in the analysis. A schematic of the side strut displacement at midspan is shown in the right hand figure. The large deflection of the side strut greatly constricts the flow passage between the struts. The constriction will alter the aerodynamic flow characteristics, most likely resulting in coupled-interaction between the flow and the strut.

DEFORMATIONS DUE TO UNSTART PRESSURE

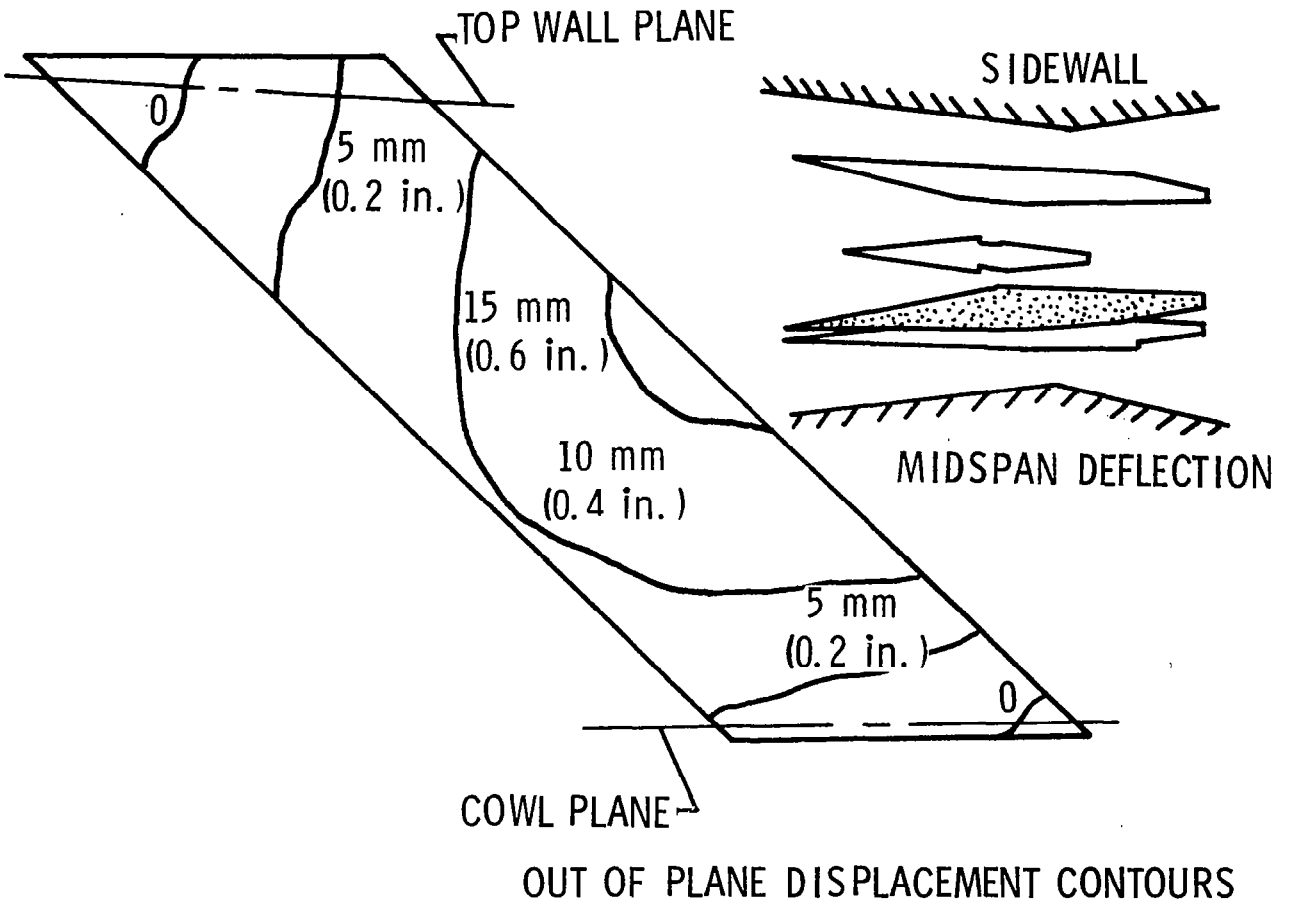

Figure 10

DYNAMICS

(Figure 11)

A feasible thermal/structural strut concept has been identified based on static loads; however, the response of this concept to potential dynamic loads has not been investigated. A cursory look at flutter indicated a factor of safety of three on flutter speed. The dynamic response of the strut to time varying pressure loads such as inlet/combustor instabilities, shock boundary-layer interactions, and the unstart transients needs to be determined; however, the dynamic characteristics of these loads have not been sufficiently defined. A preliminary vibration analysis of the strut indicates a first mode (bending) frequency of 170 Hz which is potentially within the range of engine time varying loads and indicates the possibility of large dynamic deformations and stresses.

DYNAMICS

- FLUTTER - FACTOR OF SAFETY OF 3 ON FLUTTER SPEED
- TIME VARYING LOAD CHARACTERISTICS UNDEFINED
  - INLET/COMBUSTOR INSTABILITIES
  - SHOCK BOUNDARY-LAYER INTERACTIONS
  - UNSTART TRANSIENT
- VIBRATION ANALYSIS SHOWS FUNDAMENTAL FREQUENCY OF 170 Hz
- KNOWLEDGE OF DYNAMIC RESPONSE REQUIRED

Figure 11

CONCLUDING REMARKS

(Figure 12)

Results of a thermal-structural design analysis study of a fuel-injection strut for a NASA concept of an airframe integrated hydrogen-cooled scramjet indicate a feasible thermal/structural concept has been identified for the static load conditions. Thermal stresses dominate the static response. Potentially critical dynamic loads exist and consequently a knowledge of the dynamic response is required to finalize the design. However, the basic design has progressed sufficiently to warrant development of fabrication processes and testing of flight hardware to verify the thermal/structural performance.

CONCLUDING REMARKS

- FEASIBLE THERMAL/STRUCTURAL CONCEPT IDENTIFIED FOR STATIC LOADS
- THERMAL STRESS DOMINATES STATIC RESPONSE
- KNOWLEDGE OF DYNAMIC RESPONSE REQUIRED
- NEED HARDWARE AND TESTS TO VERIFY FABRICATION AND PERFORMANCE

Figure 12

REFERENCES

1. Jones, Robert A.; and Huber, Paul W.: Airframe-Integrated Propulsion System for Hypersonic Cruise Vehicles. Recent Advances in Structures for Hypersonic Flight, NASA CP-2065, 1978. (Paper no. 3 of this compilation.)

2. Wieting, Allan R.; and Guy, Robert W.: Thermal-Structural Design/Analysis of an Airframe-Integrated Hydrogen-Cooled Scramjet. AIAA Journal of Aircraft, vol. 13, no. 3, Mar. 1976, pp. 192-197.

3. Staff of Langley Research Center and AiResearch Manufacturing Co., The Garrett Corp.: Hypersonic Research Engine Project Technological Status 1971. NASA TM X-2572, 1972.

4. Buchmann, O. A.: Design and Analysis of a Scramjet Engine. Recent Advances in Structures for Hypersonic Flight, NASA CP-2065, 1978. (Paper no. 5 of this compilation.)

5. Wieting, Allan R.: Exploratory Study of Transient Unstart Phenomena in a Three-Dimensional Fixed-Geometry Scramjet Engine. NASA TN D-8156, 1976.

6. Kelly, H. Neale; Wieting, Allan R.; Shore, Charles P.; and Nowak, Robert J.: Recent Advances in Convectively Cooled Engine and Airframe Structures for Hypersonic Flight. Recent Advances in Structures for Hypersonic Flight, NASA CP-2065, 1978. (Paper no. 4 of this compilation.)